Journal of Nuclear Materials 623 (2026) 156465

Contents lists available at ScienceDirect

Journal of Nuclear Materials

journal homepage: www.elsevier.com/locate/jnucmat

Corrosion of metallic beryllium in various aqueous solutions

Andrey Bukaemskiy [a,*], Guido Deissmann [a], Sebastien Caes [b], Giuseppe Modolo [a], Dirk Bosbach [a]

[a] Forschungszentrum Jülich GmbH, Institute of Fusion Energy and Nuclear Waste Management (IFN-2), Wilhelm-Johnen Straße, 52428 Jülich, Germany
[b] Belgian Nuclear Research Centre (SCK CEN), Institute for Sustainable Waste & Decommissioning, Boeretang 200, B-2400 Mol, Belgium

HIGHLIGHTS

- Corrosion of beryllium was studied in NaOH and simulated OPC and MPC solutions.
- New method for corrosion kinetics evaluation is proposed.
- The method is based on sample weight loss and solution composition measurements.
- Pitting corrosion of Be is an important mechanism under studied conditions.
- Only minor difference between the corrosion rates in OPC and MPC solutions is seen.

ARTICLE INFO

Keywords:
Metallic beryllium
Pitting corrosion
Corrosion rate
Microstructure
Waste encapsulation matrices

ABSTRACT

Beryllium metal is characterized by its unique physical properties, which determines its wide range of applications, including the use in nuclear reactors, resulting inevitably in activated metallic beryllium that has to be treated as radioactive waste. In the present work, the corrosion behavior of metallic beryllium in aqueous NaOH solutions with pH ranging between 6.7 and 14.0 and in solutions simulating the environment in potential waste encapsulation matrices such as Ordinary Portland Cement (OPC) or magnesium phosphate cement (MPC) was studied in detail. Corrosion rates of metallic beryllium samples were experimentally studied by using two direct methods based on gravimetric measurements and the determination of beryllium concentrations in the solution by using Inductively Coupled Plasma - Mass Spectrometry (ICP-MS). A combined method based on these two direct methods is proposed to enable the determination of corrosion rates in various aqueous solutions, including alkaline solutions and those with near neutral pH values. Detailed studies of corroded metal surfaces were carried out using scanning electron microscopy (SEM) combined with energy dispersive X-ray spectroscopy (EDS), indicating pitting corrosion as prominent corrosion mechanism.

1. Introduction

Metallic beryllium is characterized by unique physical properties such as high specific heat, high thermal conductivity, low density, and high melting point, good mechanical properties at elevated temperatures, low neutron-capture cross section, and high potential for elastic neutron scattering. This set of properties defines a wide range of applications of beryllium, for example, as moderator, reflector, or fuel cladding in thermal nuclear reactors [1–3], as the potential material for future fusion power reactors (e.g., as first wall) [4–6], as the structural material for gyroscopes and other precision navigation systems in aircraft and aerospace industries [1,7].

During utilization in fission and fusion reactors, neutron irradiation of metallic beryllium or beryllium compounds leads to formation of significant amounts of short- and long-lived activation products from neutron capture (e.g., ^{3}H formed from ^{9}Be via ^{9}Be(n,α)^{6}He → ^{6}Li(n,α)^{3}H, and ^{10}Be, as well as activation products of impurity elements, such as ^{14}C, ^{41}Ca, ^{60}Co, and ^{239}Pu). One strategy for the safe management of low- and intermediate-level radioactive metallic wastes is their encapsulation in cementitious matrices such as Ordinary Portland Cement (OPC), calcium aluminate cements or magnesium phosphate cements (MPC) [8–10]. However, reactive metals such as aluminium, magnesium or beryllium may react with cement hydration phases or the pore water under alkaline conditions, leading to detrimental effects on the

* Corresponding author.
E-mail address: a.bukaemskiy@fz-juelich.de (A. Bukaemskiy).

https://doi.org/10.1016/j.jnucmat.2026.156465
Received 15 October 2025; Received in revised form 15 January 2026; Accepted 16 January 2026
Available online 17 January 2026

conditioning matrices [11]. One major issue in this context is the formation of hydrogen gas due to metal corrosion, which might result in crack formation and gas driven transport of radionuclides out of the waste packages, impairing the confinement of the radionuclides. However, data on the corrosion and reactivity of metallic beryllium under conditions relevant to the geological disposal of radioactive wastes is scarce [12] and became only available recently (e.g. [12–14]. Thus, an analogous behaviour to aluminium had been assumed in some cases in the past [15].

Beryllium has a high affinity for oxygen and a thin (3 – 10 nm) protective oxide film forms on the metal surface in dry air atmosphere [16]. This oxide film is in a state of compression, since the volume occupied by the oxide is 1.68 times that of the metal used to form the oxide (Pilling–Bedworth ratio). Thus, the oxide layer formed on the surface of beryllium has no tendency for cracking or spalling and decreases interdiffusion and chemical interaction between the metal and the environment [16]. This determines the high corrosion resistance of beryllium. Therefore, literature data on direct measurements of beryllium corrosion rates in aqueous solutions are rather outdated and scarce and apparently estimates rather than accurately measured values [17, 18]. In recent publications, direct determinations of the corrosion rate were performed by measuring the hydrogen release [14] and by combining weight loss measurements and solution chemistry [15], respectively, the latter continued in this work. It should be noted that the results obtained in both studies correlate well with each other.

The physico-chemical aspects of the passivation and degradation of metallic beryllium in aggressive media such as NaCl and KCl have been investigated by various authors using different electrochemical methods such as open circuit potential (OCP) measurements and electrochemical impedance spectroscopy (EIS) [19–25]. These methods allow to study in detail the kinetics and mechanisms of corrosion; however, the determination of important characteristics such as the corrosion rate (implying the mass change of the corroded metal pro time) is not possible or is problematic, requiring many assumptions.

Recently, within the context of the disposal of radioactive reactive metals, the reactivity of beryllium in aqueous solutions from acidic to basic pH was studied in detail [12,13]. Based on experimental data (pH, OCP and EIS) and thermodynamic calculations, a solubility diagram was constructed, and the stability regions of various forms of beryllium were determined. It was shown that the metal surface is passivated in a wide pH range from 6 to 14 due to the formation of a surface layer of beryllium hydroxide. In addition, the passivation of (metallic) beryllium strongly depends on its concentration in solution.

In this paper, the corrosion behavior of metallic beryllium in aqueous NaOH solutions (pH range from 6.7 to 14.0) and in solutions simulating the pore solutions of potential waste encapsulation matrices such as OPC or MPC were examined in detail, including the analysis of microstructural factors. Corrosion rates of metallic beryllium samples were determined experimentally by using combined method based on gravimetric measurements (mass loss) combined with the determination of beryllium concentrations in solution. Moreover, detailed studies of pristine and corroded metal surfaces were carried out providing insights into corrosion mechanisms and the possible initiation places for pitting corrosion in dependence on the solution composition. The aim of these investigations was to study beryllium corrosion under well-controlled conditions to generate data on corrosion kinetics and gain insights into benefits or detriments of using different encapsulation matrices for metallic beryllium regarding corrosion and H_2 generation.

2. Materials and methods

2.1. Initial material and samples preparation

Beryllium foil (Alfa Aesar, 99.8 % purity) was used in as received condition. For the corrosion experiments no additional mechanical treatments, such as polishing, were carried out. The density of the Be foil was measured by hydrostatic weighing in water (Archimedes method) and equals 1.842 ± 0.001 g/cm^3, correlating well with reference data [26]. The thickness of the foil was measured with a micrometer (Digital Indicator ID-N/ID-B) at ten points and is equal to 248 ± 2 μm. For experiments on metal corrosion, Be samples with a size of approximately 1.7 cm x 3.2 cm were mechanically cut out. The surface area of the samples was calculated from their geometric dimensions. The initial samples were cleaned by rinsing them with acetone and ethanol and were treated with HCl (0.5 M) solution (around 1 min). Such short-time (0.5 – 1 min) acid treatments are standard procedures for preparing metallic beryllium samples prior to corrosion testing to eliminate the harmful effects of mechanical processing of samples (cutting, rolling, etc.) and to remove burrs [12,17,20]. Subsequently, the foils were rinsed thoroughly with demineralized water and dried with tissue paper.

The cross sections of the initial and corroded samples were prepared as follows. The samples were installed perpendicular to the foil plane and fixed with epoxy resin. The samples were firstly mechanical abraded using 500, 800 and 1200 SiC abrasive papers, and then polished using 1 μm diamond paste.

2.2. Corrosion tests

The corrosion experiments were carried out in tightly sealed plastic containers with a volume of 0.5 L under air atmosphere. Five NaOH solutions with pH values equal to 6.7, 12.5, 13.3, 13.4 and 14.0 were used. The solutions were prepared by addition of NaOH (Merk Millipore, >99 % purity) to the ultrapure water (pH ~ 4.7). The pH measurements were carried out with a Metrohm 827 pH meter. Calibration was performed using three Metrohm pH standard solutions with pH 4.00, 7.00, and 10.01, respectively.

Beryllium corrosion tests were also performed in solutions representative for young pore solutions of OPC, MPC and MPC with addition of boric acid (MPC+ *B*). The compositions of these solutions were recommended in [14] and are given in Table 1.

The initial volume of the solution was 250 mL. Every 1–2 days, the beryllium foils were removed from the solutions, thoroughly washed with demineralized water, dried with tissue paper and weighed, and replaced into the respective solutions afterwards. In addition, at each time step 2 mL of the leaching solutions were sampled for subsequent determination of beryllium concentrations by using Inductively Coupled Plasma - Mass Spectrometry (ICP-MS). The total duration of the corrosion experiments was 30 or 120 days.

The corrosion rate (CR) was determined by the weight loss method. According to [27], the corrosion rate (CR, μm/year) was calculated using the following equation,

$$CR(\mu m / y) = 3.65{\cdot}10^6 \frac{m_{Be}^{cor}}{\rho S t} \quad (1)$$

where (m_{Be}^{cor}) is the mass of corroded beryllium, ρ (g/cm^3) is the density of the material (1.842 g/cm^3), S (cm^2) is the total initial sample surface area, t (day) is the exposure time, and the constant $3.65{\cdot}10^6$ is used for unit conversion to μm/y.

2.3. Characterization methods

Detailed studies of the morphological features of the structure of pristine and corroded metal surfaces were carried out using a FEI model

Table 1
Composition (mol/L) and pH value of the OPC, MPC and MPC+*B* solutions.

	Na^+	K^+	SO_4	PO_4^{3-}	BO_3^-	pH
OPC	0.14	0.37	0.002	–	–	13.4
MPC	–	3.76	–	1.98	–	7.9
MPC + *B*	–	3.76	–	1.98	0.54	7.7

Quanta 200F SEM equipped with a Genesis 4000 EDS analyzer and an optical microscope ZEISS KS300. The beryllium content in solution was analyzed by Inductively Coupled Plasma - Mass Spectrometry (ICP-MS) with an NexION 2000C device by PerkinElmer. The crystal structure of the samples studied was analyzed by X-ray diffraction methods (XRD). All measurements were performed at room temperature with a D8 Advance by Bruker AXS GmbH. The surface structure of the initial sample, namely its roughness, was studied using a KLA-Tencor AlfaStep IQ Surface Profilometer.

3. Results and discussion

Fig. 1a shows the surface of the original Be foil with two types of mechanical defects visible on the surface of the beryllium metal, namely numerous elongated linear defects (scratches) due to mechanical processing (rolling) and, locally present, rather deep defects (cavities). The impurity inclusions are also present in the material as white spots in Fig. 1a, b. Size of impurity inclusions vary between 0.3 to 5 μm. These inclusions were identified by detail SEM-EDS investigation as BeO, Be_2C, silicon (Si), and various intermetallic phases such as Be/Cr/Al/Mn, Si_2Cr and Al/Mn/Si/Cr. A representative SEM image of the sample surface with compositional and dimensional characteristics of the inclusions is shown in Fig. 1b. Our results on the impurity arrangement and their dimensional and compositional characteristics are in good agreement with literature data [24,25].

The surface structure of the initial Be sample was studied on a profilometer with a measurement step equal to 0.02 μm. The representative SEM surface image of the surface and the roughness profile are shown in Fig. 2. The value of the mean square average of profile height deviations from the mean line (Rq) equals 0.17 μm. The maximum depth of some scratches can reach 2 μm, but their number is insignificant. The average spacing between scratches is 3 μm. These results make it possible to clarify the increase in the sample area due to its roughness. This value is only 1.4 % and deemed insignificant here. Therefore, surface roughness was not considered in the present work.

3.1. Corrosion of Be in NaOH solutions

Five NaOH solutions with pH values equal to 6.7, 12.5, 13.3, 13.4 and 14.0 were used. The choice of these concentrations was due to the following reasons. The solutions with a pH of 6.7 and 13.4 are close to MPC and OPC cement pore water in this parameter, respectively. A detailed study of corrosion in the pH range from 12.5 to 14 allows us to conduct a comparative analysis of corrosion processes in aluminum and beryllium (see below).

The Be corrosion rate was measured using two direct methods, namely, measurements of weight loss of the initial samples (WL) and the concentration of beryllium in solution (ICP-MS). However, the weight

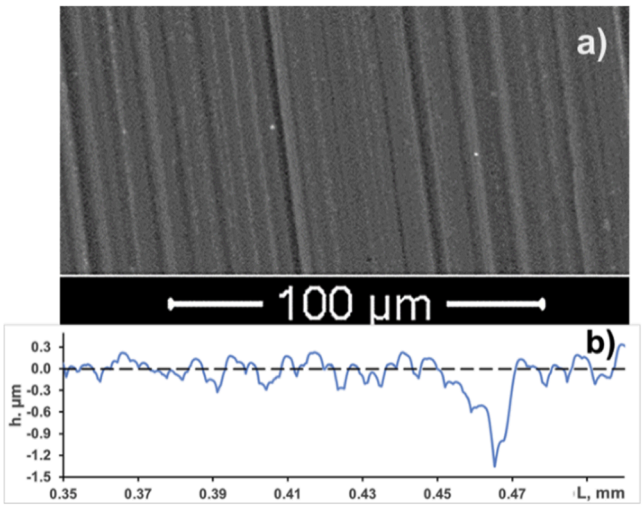

Fig. 2. Representative SEM surface image of a pristine Be-sample surface (a) and surface roughness profile (b).

loss of the samples during corrosion at near neutral conditions and at pH <13 is insignificant and is maintained at the level of experimental measurement accuracy, Fig. 3a. For example, at pH = 12.5, the change in the weight of the sample during the first three weeks remains constant and equal to zero. A slight decrease in the mass of the sample takes place only during the fourth week. For the sample under study at pH = 6.7, a slight but stable increase in weight is observed. In these cases, it is not possible to determine the corrosion rate from measurements of changes in the weight of the sample. Simultaneously, the content of beryllium in solution for all experiments is well measurable and increases with the duration of the experiment (Fig. 3b).

Ideally, the values of the corrosion rates determined by these two methods (WL and ICP-MS) should be equal. However, it has been shown that for all experiments, the corrosion rate values determined from the measurement of the beryllium content in solutions (ICP-MS) are always lower than those determined by the change in the weight (WL) of the initial samples.

This difference can be explained by the formation of a hydroxide layer on the surface of the samples during the corrosion process. This assumption is consistent with the results of the study [13] that indicates the formation of a surface layer of beryllium hydroxide in a wide pH range from 6 to 14. This is particularly evidenced by the increase in the weight of the sample during corrosion experiments at pH = 7.6, the corrosion start delays (zero mass loss) are 3 and 21 days for pH 12.5 and 13.3, respectively (Fig. 3a). The formation of a hydroxide layer at the corrosion points in these experiments is confirmed by detailed optical

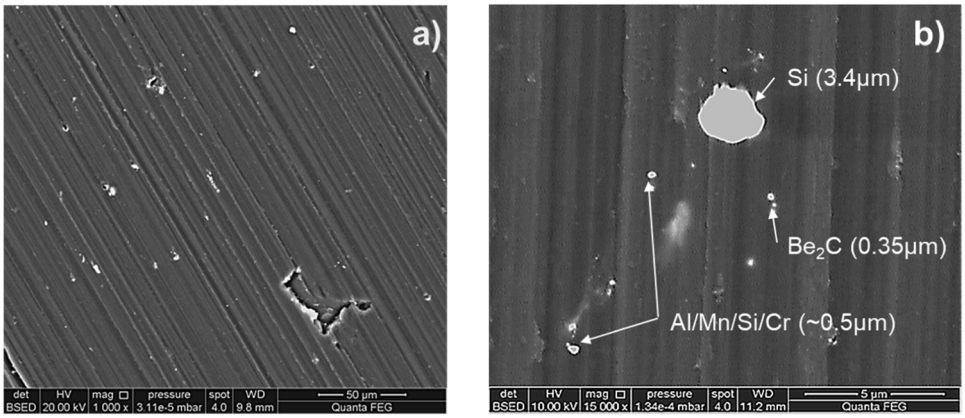

Fig. 1. SEM surface images of a pristine Be-sample surface.

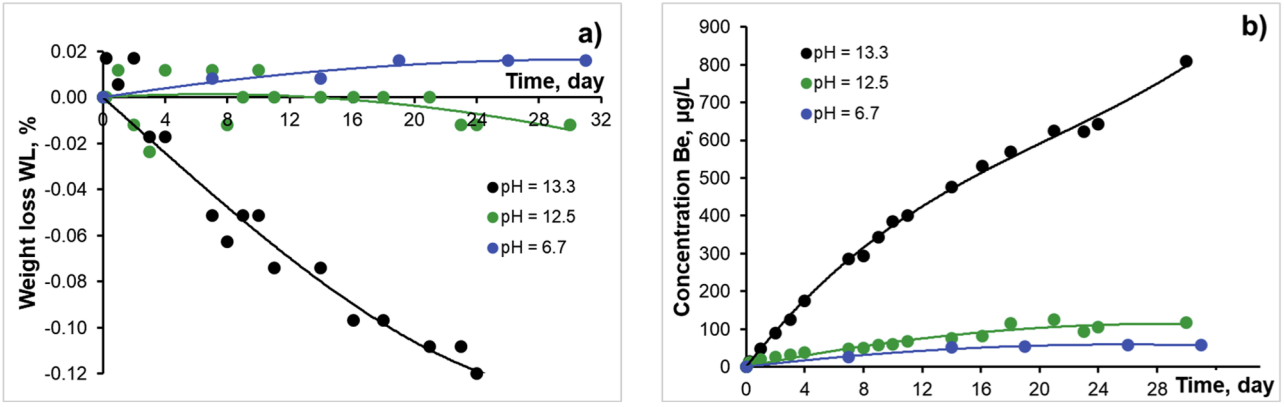

Fig. 3. (a) Sample weight loss (WL) and (b) concentration of Be in solution in experiments at pH 6.7, 12.5, 13.3 as function of exposure time.

microscope studies in normal (upper line of photographs) and polarized (lower line of photographs) light, Fig. 4.

The optical image of the initial beryllium foil surface is shown in Fig. 4a, b. The photographs clearly show elongated linear defects (scratches), three large (~ 4–6 μm) and several small impurity inclusions (black and white objects in Fig. 4a, b).

Fig. 4c, d, e, f shows the evolution of changes in the surface structure of the sample during corrosion tests at pH 14.0 for 6 days (4c, d) and 30 days (4e, f), respectively. After a six-day corrosion test, the formation of a sufficiently large hydroxide layer (~40 μm) is observed on the surface of the sample. Apparently, the formation of this layer occurs above the corroded area (corrosion pit). The elongated surface roughness structure does not change. An increase in the duration of the corrosion test to 30 days leads to a significant increase in the size of the corrosion areas (~100*50 μm), their deepening and an increase in the thickness of the hydroxide layer, Fig. 4e, f. The elongated surface roughness structure almost completely disappears.

A prolonged corrosion test (30 days) at pH values equal to 12.5 also leads to the formation of large areas of corrosion, but is not accompanied by a change in the surface structure of the sample, Fig. 4g, h.

In addition, detailed studies of beryllium and oxygen content on the corroded samples were carried out using SEM with EDS analyses. Measurements were carried out on 5–10 areas, and the average values of oxygen content and the experimental measurement error were calculated. It was shown that in the areas of the Be samples without significant changes in the surface structure, the average value of oxygen content is 6.9 ± 1.4 at. %. Apparently, in this case, the presence of oxygen is determined by the presence of a thin oxide film on the surface of the sample.

Whereas in the big corrosion areas the value of oxygen content increases by 5 times and is equal to 35.1 ± 1.3 at. %. This indicates the formation of a sufficiently thick layer of beryllium hydroxide directly above the corroded areas, as shown, for example, in Fig. 4c-f.

The stability of the hydroxide layer on the surface of the Be sample was previously discussed in [15], and it was due to the good adhesion of beryllium hydroxide to the metal surface, that was explained by

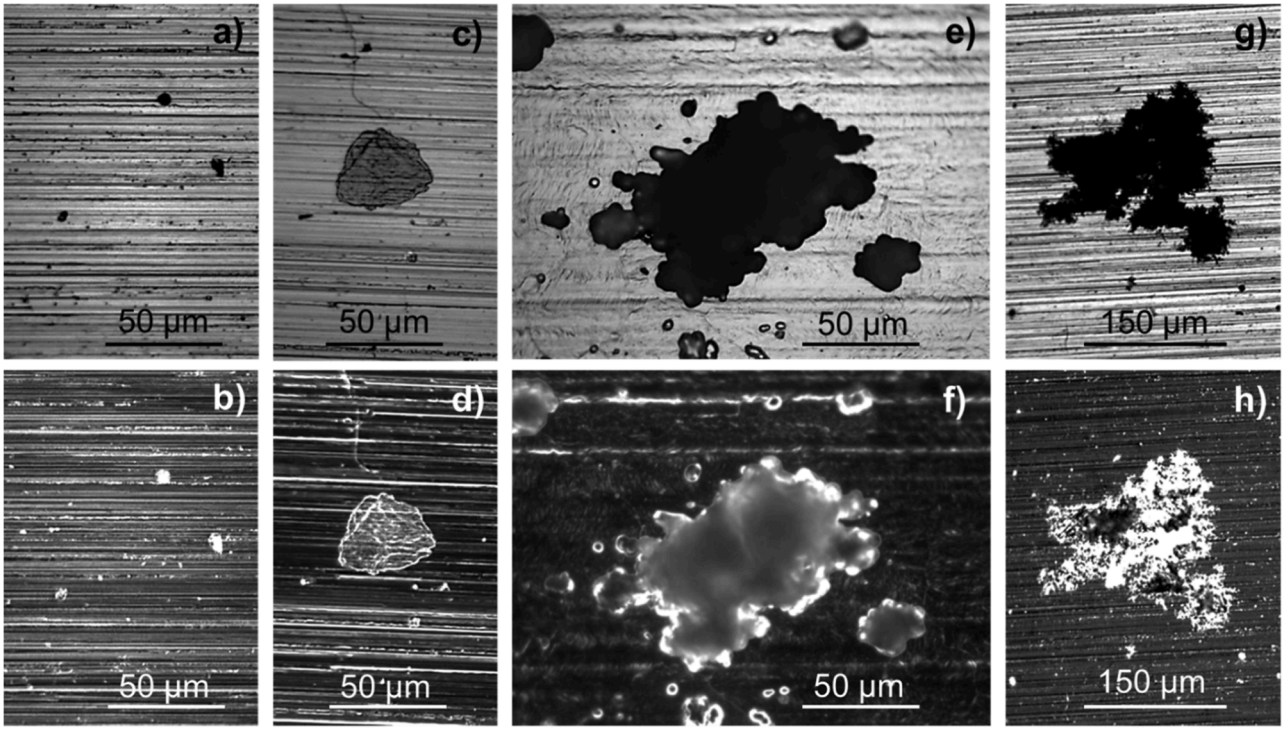

Fig. 4. Optical images of Be surface for (a, b) initial sample, sample corroded at pH 14.0 during (c, d) 6 days and (e, f) 30 days and (g, h) sample corroded at pH 12.5 during 30 days. (a, c, e, g) - normal and (b, d, f, h) - polarized light.

similarities of their crystal lattice parameters ($a_{Be} = 2.287$ Å [28] ≈ 0.25 $(a + b)_{Be(OH)2} = 2.288$ Å [29]).

Thus, the presence of a hydroxide layer on the surface of the sample should lead to a decrease in weight loss (WL) and the content of beryllium in the solution. Therefore, the values of the corrosion rate measured by these methods should be lower than the actual corrosion rate of beryllium.

The presence of a hydroxide layer on the metal surface leads to an underestimation of the amount of corroded metal by measuring WL:

$$WL = -m_{Be}^{cor} + R \cdot m_{Be}^{s} \quad (2)$$

where $\boldsymbol{m_{Be}^{cor}}$ is the mass of corroded beryllium and $\boldsymbol{m_{Be}^{s}}$ the mass of beryllium being in the form of hydroxide on the sample surface, and the coefficient $R = 4.774$ is the ratio of the molecular weight of the hydroxide and the metal.

The mass of corroded beryllium consists of two components – the mass of Be as hydroxide on the metal surface m_{Be}^{s} and that dissolved in solution (m_{Be}^{sol}).

$$m_{Be}^{cor} = m_{Be}^{s} + m_{Be}^{sol} \quad (3)$$

Using Eqs. (2) and 3, an equation (Eq. (4)) can be obtained for the mass of corroded beryllium, which consists of two experimentally measured values – the concentration of beryllium in solution (determined by ICP-MS) and the mass loss (ML).

$$m_{Be}^{cor} = \frac{R \cdot m_{Be}^{sol} + WL}{R - 1} \quad (4)$$

An example of processing experimental data on weight loss (WL) and beryllium content (ICP-MS) in solution in order to determine the corrosion rate is shown in Fig. 5 for the representative case of a corrosion experiment performed at pH = 13.4.

In Fig. 5a, the measured weight loss (WL) and concentration of beryllium in solution (ICP-MS) are shown for a representative experiment performed at pH = 13.4 as function of experimental duration. The mass of the sample decreases (brown line), whereas the Be content in solution (blue line) increases monotonically with increasing duration of the experiment. Based on these data, the corrosion rates (CR) were calculated; the results are presented in Fig. 5b (brown and blue lines, respectively). The average values of corrosion rates and their experimental errors were calculated specifically for the last three experimental points and is equal to 5.01 ± 0.11 μm/y and 3.56 ± 0.08 μm/y, respectively.

The evolution of the beryllium corrosion rate, taking into account the presence of a hydroxide layer (Eq. (3)), is shown in Fig. 5b (red line). The value of the average corrosion rate after 30 days is 5.83 ± 0.13 μm/y. The corrosion rate determined by our combined method is higher than those determined by the direct measurements (WL and ICP-MS). Indeed, in the case of weight loss measurements, the increase in the weight of the sample due to the presence of a hydroxide layer on the surface of the sample is not taken into account. Similarly, the beryllium content in the solution also does not take into account the beryllium contained in this layer.

It should be particularly noted that the proposed combined method makes it possible to determine the low corrosion rates of beryllium at pH equals 7.6 and 12.5 when the change in the mass of the sample is close to zero or even positive, see Fig. 3a. That is, even in cases where measuring the corrosion rate solely by the WL method is impossible.

In Fig. 6a, the measured weight loss (WL) and concentration of beryllium in solution (ICP-MS) are shown as function of experimental duration at pH = 6.7. The weight of the sample (brown line) and the Be content in the solution (blue line) increase monotonously during the first 30 days and then remain unchanged. It should be specifically noted this "abnormal" (increasing) behavior of the dependence of weight loss on the time of the experiment. This indicates that the weight of the formed hydroxide layer on the surface of the sample exceeds the mass of the corroded beryllium. Apparently, during the first 30 days, the defective areas (scratches, cavities, impurities) on the surface of the material are actively corroded. These areas are covered with a protective layer of hydroxide, as shown for example in Fig. 4c, d. As a result, the corrosion process slows down significantly after 30 days. This type of weight loss dependence does not allow us to determine the rate of corrosion. However, the corrosion rate can be calculated from the results of measuring the beryllium content in solution, the blue line in Fig. 6b. The combined technique proposed allows us to consider the presence of a hydroxide layer (Eq. (4)). The evolution of the beryllium corrosion rate in solutions with a low pH = 6.7 is shown in Fig. 6b (red line). The values of the average corrosion rate after 30 and 120 days are 0.16 ± 0.01 μm/y and 0.040 ± 0.002 μm/y, respectively.

The results of the corrosion rate measurements (duration 30 days) at various pH values are summarized in Table 2.

According to [16], the high corrosion resistance of beryllium metal is due to the presence of a thin oxide film on the metal surface. The actual corrosion of beryllium metal begins at sensitive locations where the integrity of the oxide film is compromised, namely on crystallographic defects, cavities, or scratches in the metal surface and/or impurity inclusions mainly localized along grain boundaries [19,23,24].

Fig. 7a shows a representative SEM image of the corroded Be metal surface. Two types of corrosion pits could be observed in the corroded samples: large (40 – 200 μm) and small (4 – 30 μm) pits. For each sample from five SEM micrographs (total area of 7 mm^2) the characteristic size of the corroded pits was measured. Based on these measurements, the size distribution of corrosion pits was determined as shown in Fig. 7b for the case of Be corrosion at pH 12.5 for 30 days. The size distribution of

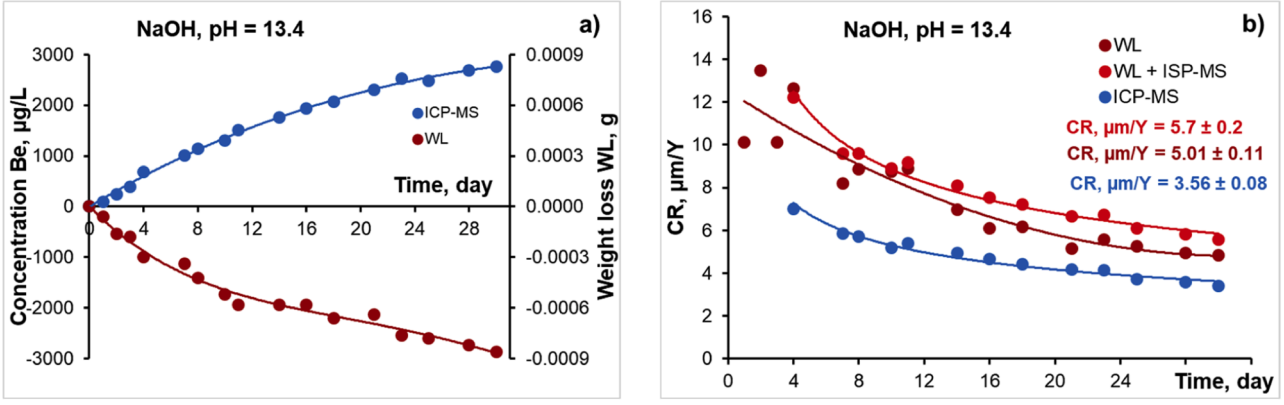

Fig. 5. (a) Sample weight loss (ML) and concentration Be in solution in representative experiment at pH 13.4, as function of exposure time, (b) corrosion rate measured by 3 methods (WL, ICP-MS, WL+ICP-MS) as function of exposure time.

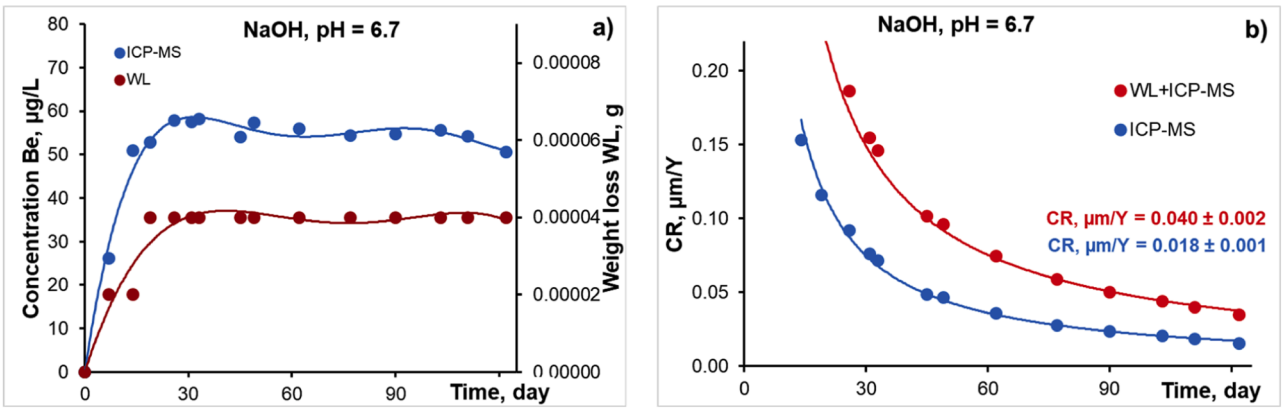

Fig. 6. a) Sample "abnormal" mass loss (WL) and concentration Be in solution at pH 6.7, as function of exposure time, b) corrosion rate measured by 2 methods (ICP-MS, WL+ICP-MS) as function of exposure time.

Table 2
Corrosion rates (CR) of metallic beryllium in NaOH solutions of different pH.

Medium	pH	CR, µm/y
NaOH	6.7	0.16 ± 0.01
NaOH	12.5	0.18 ± 0.01
NaOH	13.3	2.47 ± 0.02
NaOH	13.4	5.7 ± 0.2
NaOH	14.0	189 ± 1

all corrosion pits (red line) consists of the sum of two lognormal distributions corresponding to large (green line) and small (blue line) pits. The virtual boundary between large and small particles ($d_{c\text{-}f} \sim 29$ µm) is shown in Fig. 7b by a red dotted vertical line.

The results of this processing of the size distributions of corrosion pits for samples corroded at different pH are summarized in Table 3, where d_c, d_f are the average size of the large and small pit fractions, respectively; N is the total number of corrosion pits per unit area (square centimeter) as well as N_c and N_f are the numbers of large and small pits, respectively. It can be seen that the main distribution characteristics (d_c, d_f and $d_{c\text{-}f}$) are similar for cases of beryllium corrosion at pH equal to 12.5 and 13.3. However, with an increase in pH to 14.0, the average size of the fine fraction and the boundary size increases twice, whereas the average size of a large fraction increases slightly.

As can be seen from Table 3 and Fig. 8, the total number of corrosion pits increases monotonously (by 5 times) with increasing pH. This increase is mainly determined by an increase in the number of small corrosion pits. Whereas the number of large corrosion pits increases only slightly (factor 1.6) from pH 12.5 to 14.0.

Thus, the large corrosion pits are formed at all solution pH values. Their size and quantity increase slightly with increasing pH. Therefore, we can assume that the formation of large corrosion pits occurs mainly on cavities and on the large scratches that are present in the original foil, Fig. 1a.

Representative SEM photographs of the foil surface after corrosion tests for 30 days at pH 13.3 and pH 14.0 are shown in Fig. 9a, b. It can be seen that both large and small corrosion pits are present on the surface. Also in Fig. 9a, e, f, g the characteristic preserved longitudinal scratches of the initial material are clearly visible. This indicates a slight corrosion of the foil surface and a predominant corrosion of the material in the problem areas - cavities and the edge of scratches at pH below 13.3. At high pH = 14.0, longitudinal scratches are not observed on the foil surface, Fig. 9b, c, d, h, i. Also, this indicates a significant dissolution of the sample surface.

The SEM analyses show large corrosion pits that are not hemispherical and have an irregular shape with a complex internal morphological structure, Fig. 9 c-f. The pits consist of several special areas with differently oriented parallel plates as indicated by white

Table 3
Main characteristics of the size distributions of corrosion pits for different pH.

pH	d_c, µm	d_f, µm	$d_{c\text{-}f}$, µm	N, cm^{-2}	N_c, cm^{-2}	N_f, cm^{-2}
12.5	44.7	7.9	29	1579	725	854
13.3	44.7	6.1	28	2631	782	1849
14.0	89.0	11.9	61	7708	1194	6514

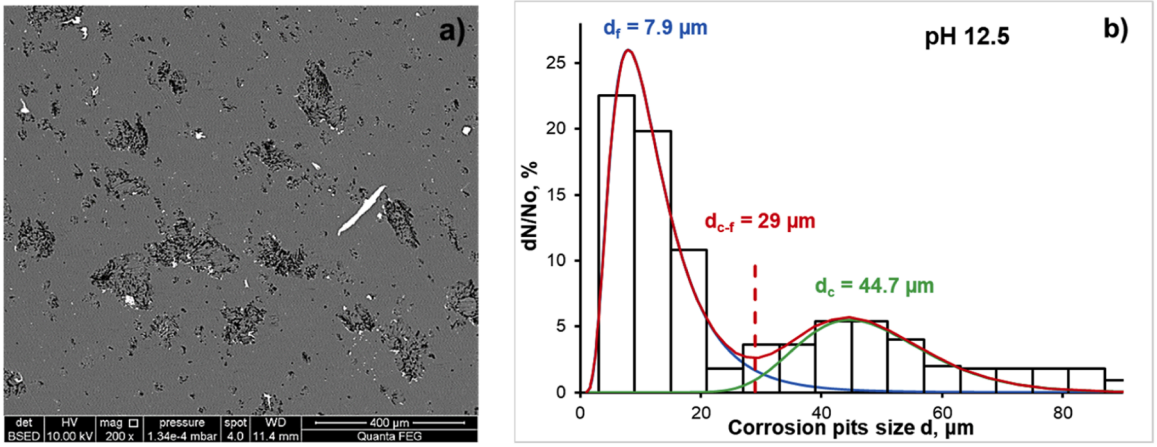

Fig. 7. a) Representative SEM surface image of a Be sample corroded for 30 days at pH 14.0, b) size distribution of corrosion pits.

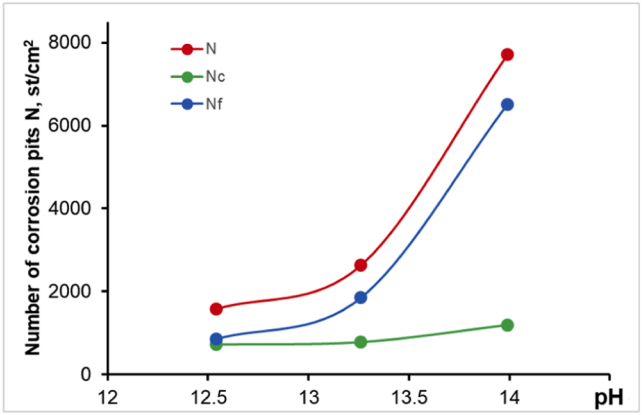

Fig. 8. Dependencies of the total number of corrosion pits (N) and the numbers of large (N_c) and small (N_f) pits, respectively, per unit area on pH.

dashed lines (Fig. 9c, d). Fig. 9d shows a large corrosion pit at higher magnification with two different morphologies corresponding to a family of spherical pits and pit walls, cf [19,22–25].

This type of large corrosion pits was previously observed in the study of corrosion of polycrystalline beryllium in sodium and potassium chlorate solutions using the electrochemical polarization method [19, 24,25]. It has been suggested that these morphological features of large corrosion pits may be related to different crystallographic orientation of the material [19].

The morphological features of the corrosion pits can be explained by varying dissolution rates of different crystallographic orientations of the Be grains [22,23]. Lillard [23] studied in detail the dissolution process of beryllium single crystals and the morphological features of the formed corrosion pits. It has been shown that the pitting potential of beryllium single-crystals in 0.01 M sodium chloride decreased with crystallographic orientation in the order $(0001) > (10\bar{1}0) > (11\bar{2}0)$. Orientations associated with the lowest pitting potential, $(10\bar{1}0)$ and $(11\bar{2}0)$, were characterized by crystallographically oriented parallel plates of unattacked Be on the pit interior and pit walls, cf [22,23]. While the surface (0001) is characterized by a generally round shape of the pits, the corrosion propagation was often in the $\langle 10\bar{1}0\rangle$ and $\langle \bar{1}2\bar{1}0\rangle$ families of

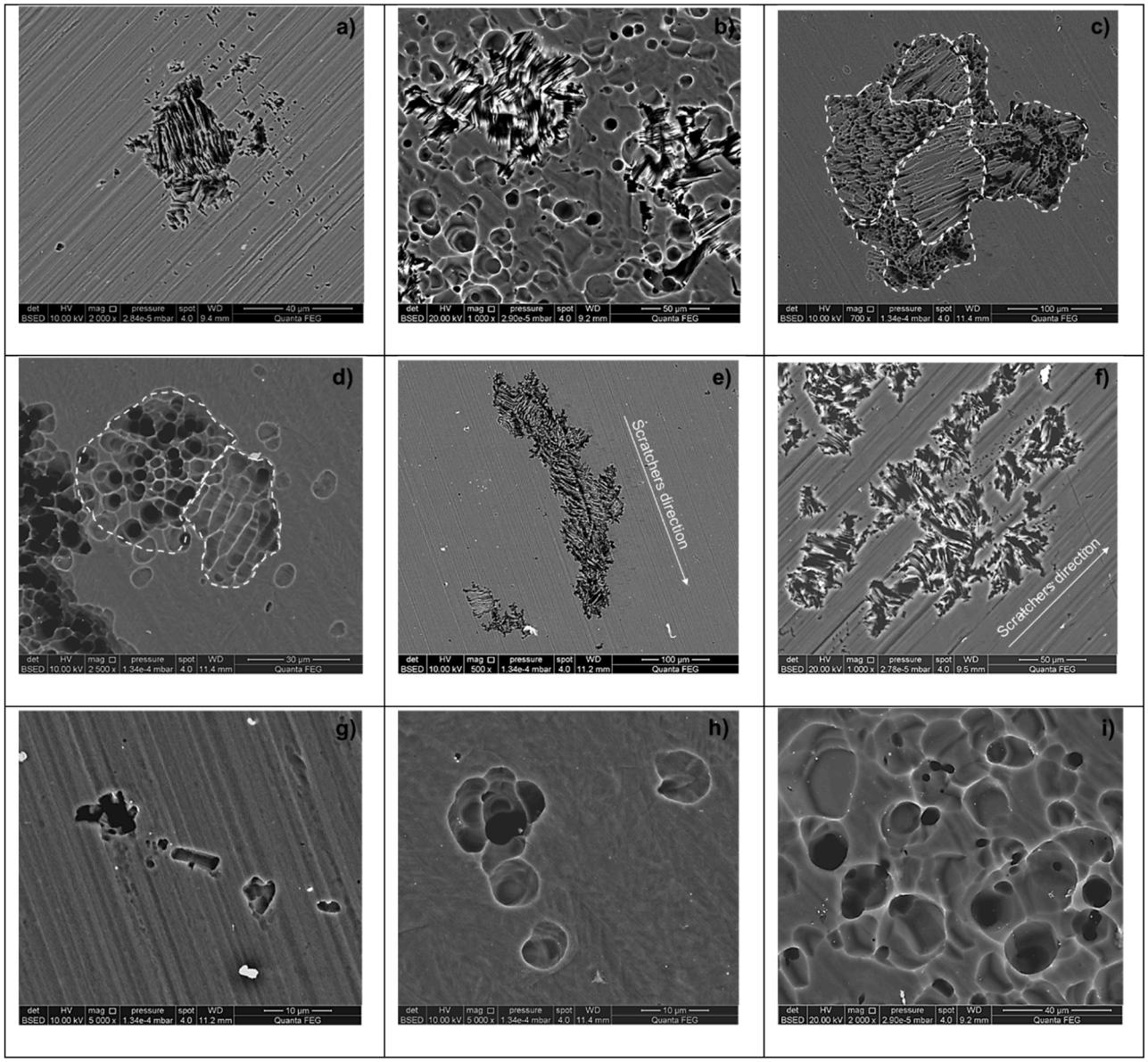

Fig. 9. SEM images of corrosion pits.

directions.

In addition, some corrosion pits have an elongated shape where the direction of pit elongation coincides with the direction of the original scratches, Fig. 9e, f. This indicates that mechanical defects (cavities, edges of scratches) in the initial beryllium foil are the initiation places for pitting corrosion.

The small corrosion pits are characterized by a spherical (cylindrical) shape, Fig. 9g, h, i. The small corrosion pits are also located on the tops of scratches and irregularities of the original Be metal, Fig. 9g.

In several studies [19,25,22], it was suggested that the size of the special areas in large corrosion pits is determined by the grain size of the original beryllium foil. In the present work, to test this hypothesis, the areas with differently oriented parallel plates in large corrosion pits were outlined as shown for example in Fig. 9c, d and their size was measured. Based on the study of 25 large corrosion pits, 312 special areas (No) were measured and the results are shown in Fig. 10 as black columns and line. It can be seen that the size of the areas with differently oriented parallel plates follows a Gaussian distribution with an average size of these areas equal to 33 ± 5 μm. In addition, the grain size was measured, and the results are also shown in Fig. 10 as red columns and line. It can be seen that the grain size distribution is also a Gaussian expansion with an average size of 31 ± 4 μm. This confirms that the size of the special areas in the large corrosion pits is determined by the grain size of the initial Be foil.

Exemplarily, a SEM image of a cross section of Be sample corroded at pH 14.0 for 30 days is shown in Fig. 11a. Based on SEM images, the average thickness of the corroded samples was determined. The results are shown in Fig. 11b as function of pH. The red dotted line corresponds to the thickness of the original sample. It can be seen that at pH <13.3, the thickness of the samples does not change within the timeframe of the experiment. At pH of 13.4, there is a slight (up to 2.5 μm) decrease in the thickness of the corroded sample. At high pH (14.0), there is a significant decrease up to 22.5 μm in the thickness of the Be foil. Also in Fig. 11a, the large corrosion pits are clearly visible, with a depth reaching 15–20 μm.

In addition, the thickness of the corroded layer can be estimated from the value of the corrosion rate (CR), see Table 2. The experimentally determined corrosion rate at a pH of 14.0 is 189 μm/y. Hence, the thickness of the corroded layer after the test for 30 days is 15.75 μm, which corresponds to a decrease in the thickness of the foil by 15.75×2 = 31.5 μm. This value is slightly higher than the one previously determined (22.5 μm) from the SEM images. Presumably, this slightly higher value of surface retreat calculated from the overall corrosion rate is caused by the presence of large corrosion pits in the material (cf. Fig. 11a).

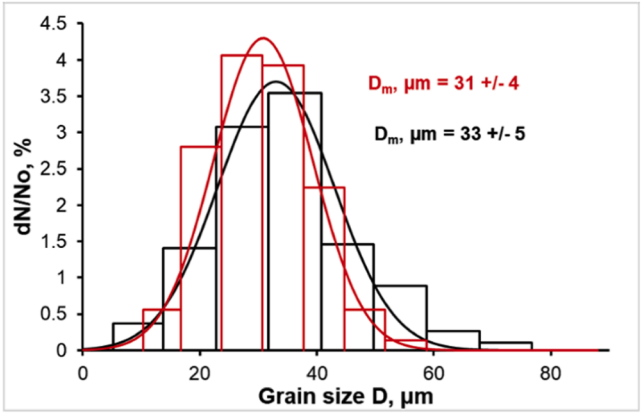

Fig. 10. Grain size (No = 102, red columns and line) and special areas size distributions (No = 312, black columns and line).

3.2. Corrosion of Be in OPC and MPC pore waters

3.2.1. Corrosion of Be in OPC pore water

The appearance of the samples after corrosion tests during 120 days in NaOH solution (pH 13.4) and in synthetic OPC pore water (pH 13.4) is shown in Fig. 12a and b, respectively. There are no significant visual changes compared to the original Be foils.

In Fig. 13a, the measured weight loss and the concentration of beryllium in solution are shown as function of experimental duration for the experiment performed in Ordinary Portland Cement pore water (pH = 13.4). The weight of the sample decreases (brown line) and the beryllium content in solution (blue line) increases monotonically with increasing duration of the experiment. Based on these data, the corrosion rates (CR) were calculated by the combined method (WL and ICP-MS); the results are presented in Fig. 13b (black line). The corrosion rates are 4.8 ± 0.2 μm/y and 1.90 ± 0.09 μm/y, for an experimental duration of 30 and 120 days, respectively.

For comparison, Fig. 13b also shows the dependence of the beryllium corrosion rate for a NaOH solution with a pH of 13.4 (red line). At similar pH values, the corrosion rate of beryllium in an OPC pore solution is slightly lower than in NaOH based solution for an experimental duration of 120 days.

3.2.2. Corrosion of Be in MPC and MPC+B pore waters

The appearance of the samples after corrosion tests in the MPC pore water (pH = 7.9) and the magnesium phosphate cement pore water with the addition of boric acid (MPC+B solution, pH = 7.7) are shown in Fig. 12c and d, respectively. It can be seen that during the corrosion process, a layer of black or grey material is formed on the surface of the Be foils, which is more prominent for the beryllium sample corroded in MPC pore solution.

In Fig. 14a, the measured weight changes (WC) are shown as function of experimental duration for experiments performed in MPC and MPC+B pore water. For both experiments, the weight of the sample first decreases, and then increases monotonically with increasing duration of the experiment. The most significant increase was observed for the sample tested in MPC pore water (Fig. 14a). The minimum weight of the sample is observed after 40 days with a WC of - 0.0004 g, then the weight of the sample increased distinctly by 0.004 g at the end of the test (brown line). For the sample tested in MPC+B pore water, the minimum in the weight is observed after 60 days (value -0.004 g) followed by a slight increase in the sample weight (black line). It is logical to assume that the increase in the weight of the samples in the later stages is due to the growth of the surface cover layer (cf. Fig. 12c, d).

Thus, it can be assumed that the measured weight change (WC) consists of two components, namely, a decrease in weight due to corrosion of beryllium (WL*), and an increase in mass due to the growth of the cover layer (M_{covL})

$$WC = WL^{*} + M_{covL} \quad (5)$$

The dependence of the mass of the cover layer M_{covL} on the duration of the experiment can be estimated as follows. For the corrosion test in MPC pore water the experimental data for WC (the increasing part after 40 days) is well described by the quadratic equation.

$$dM, g = A + Bt + Ct^2 \quad (6)$$

where A = -8.34 × 10^{-4}, B = -2.11 × 10^{-6}, and C = 3.36 × 10^{-7} are empirical coefficients.

Then, the dependency of M_{covL} on the duration of the experiment is given by Eq. (6) without a free term A (green line in Fig. 15a). The dependency of the mass of the corroded beryllium (WL*) on the experimental duration is determined from Eq. (5) and shown in Fig. 15a as the brown dotted line. For the corrosion test in MPC + B pore water, the results of this treatment are shown in Fig. 15b (the increasing part after 60 days; with fitting parameters A = -8.96 × 10^{-4}, B = -5.45 × 10^{-8},

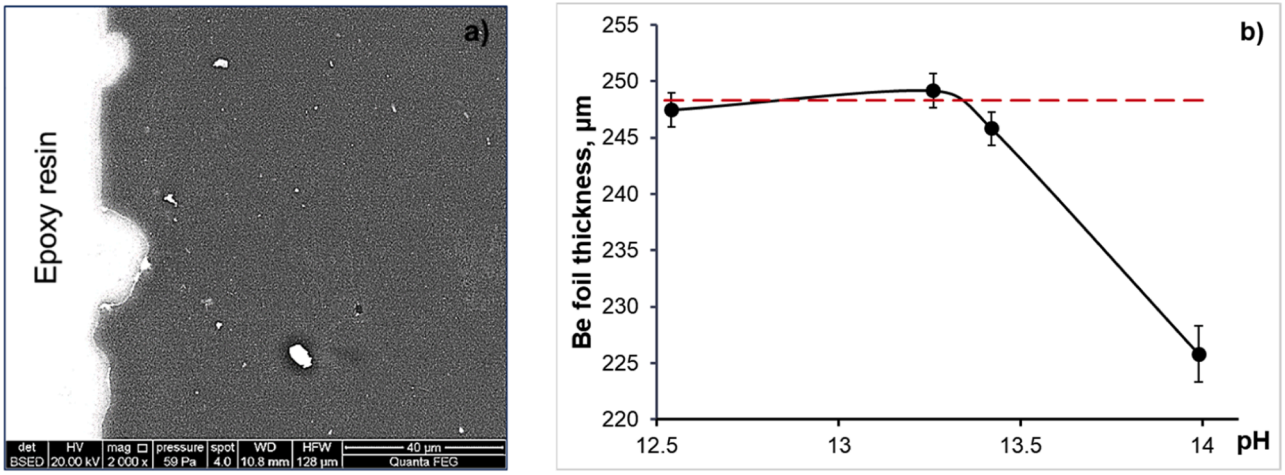

Fig. 11. (a) SEM image of transverse sections of the samples corroded at pH 14.0 (30 days); (b) dependency of the corroded Be foil thickness on pH.

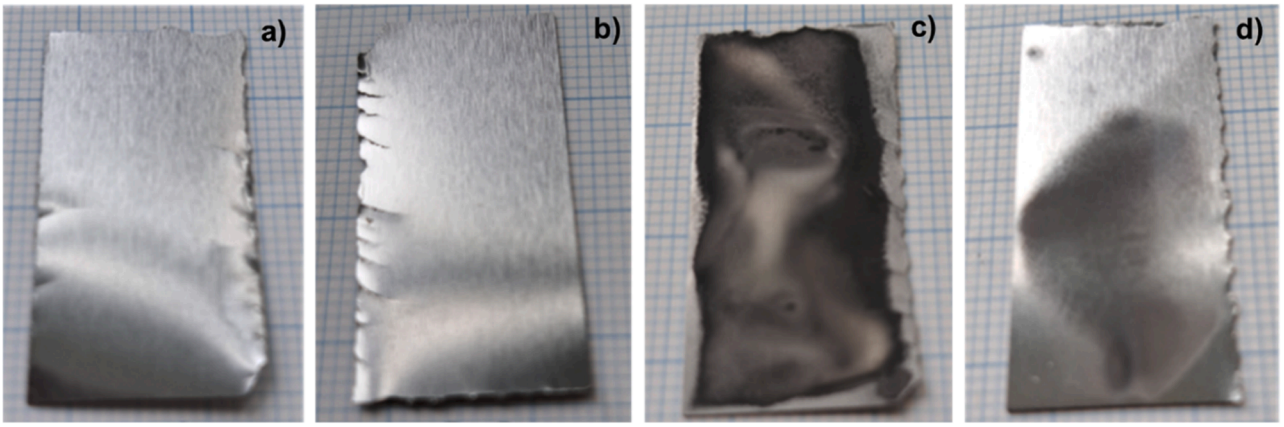

Fig. 12. Be samples after 120 days of corrosion in (a) NaOH solution (pH 13.4), (b) OPC pore water (pH 13.4), (c) MPC pore water (pH 7.9) and (d) MPC+*B* pore water (pH 7.7).

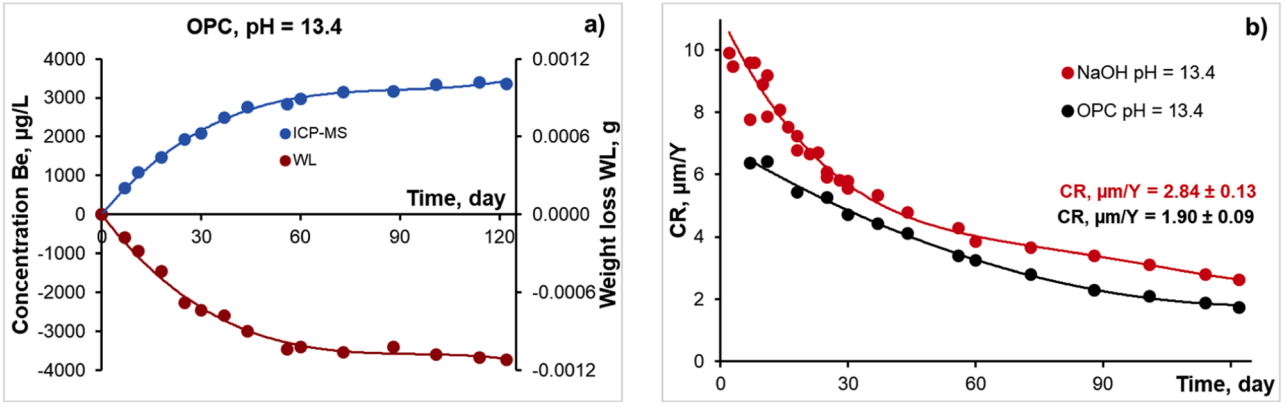

Fig. 13. (a) Sample mass loss (WL) and concentration of Be in OPC pore water as a function of exposure time, (b) corrosion rates of Be in OPC pore water and NaOH solution (pH=13.4) as a function of exposure time.

C=2.78 × 10^{-8}).

Finally, in Fig. 14b, weight loss of Be corrosion (WL*) and the concentrations of beryllium in solution are shown as function of experimental duration for experiments performed in MPC and MPC+B pore water. In both cases, the values of WL* decrease monotonously and are close to each other. Whereas the beryllium content in solutions increases monotonically, but the beryllium content in the MPC solution is about two times higher than in the MPC+B solution.

In order to understand the composition and morphological structure of the surface layer on the corroded Be foils, the surface covered layer was studied in detail using SEM and XRD. The results of the SEM examination of the Be sample after a corrosion test in MPC solution for 120 days are shown in Fig. 16.

It has been shown that the morphological structure of the surface

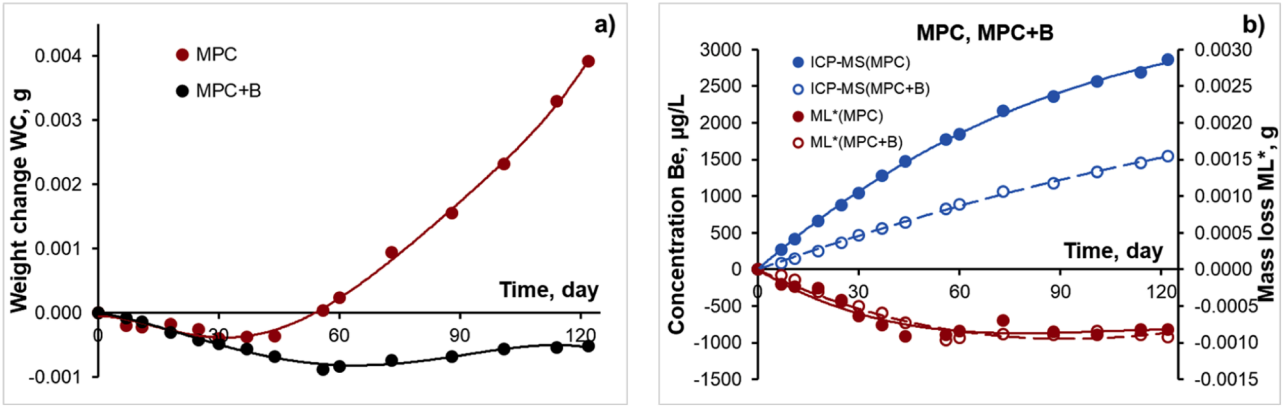

Fig. 14. (a) Sample weight change (WC) and (b) sample weight loss (WL*) and concentration Be in MPC and MPC+*B* pore water as a function of exposure time.

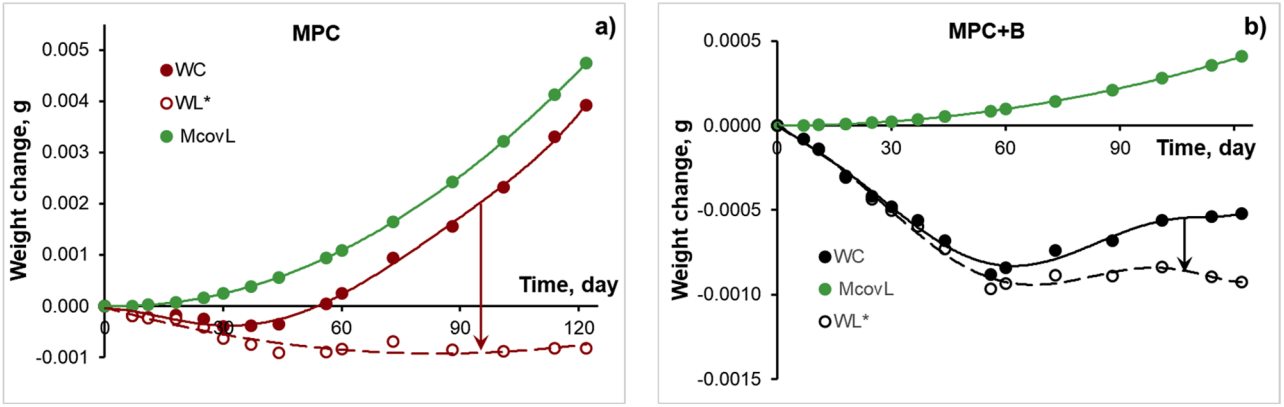

Fig. 15. Sample weight change (WC) splitted into beryllium mass loss (WL*) and covered layer mass (M_{covL}) as a function of experimental duration for corrosion experiments in (a) MPC and (b) MPC + *B* pore waters.

covered layer depends on its thickness. The thin layer consists mainly of randomly oriented needle-like crystals, Fig. 16a. The crystals have a square shape in cross-section, the average size is 0.23 ± 0.02 µm. The average ratio of crystal length to cross-sectional size is 8 ± 1. However, for some crystals, this ratio reaches 18. In addition, particles of regular elliptical shape with an average size of 0.41 ± 0.06 µm are also observed in Fig. 16a. The average aspect ratio equals 1.7 ± 0.1. These types of particles are located directly on the surface of the beryllium sample and are probably the nuclei of the coating-forming phase.

The thick subsurface cover layer is characterized by the needle-like crystals of square cross section with the predominant orientation of perpendicular to the surface of the Be sample (the columnar structure), Fig. 16b The cross-sectional size of crystals increases significantly up to 0.63 ± 0.06 µm compared to needle-like crystals in a thin layer.

To study the mineralogical composition of the surface cover layer, a part of this layer was mechanically scraped off and then examined by X-ray diffraction, Fig. 17.

It has been shown that the covered layer consists mainly of the compound $BeKPO_4{\cdot}H_2O$ (Fig. 17, red diamonds according to the catalog data 00–019–0939) with an orthorhombic crystal structure, which

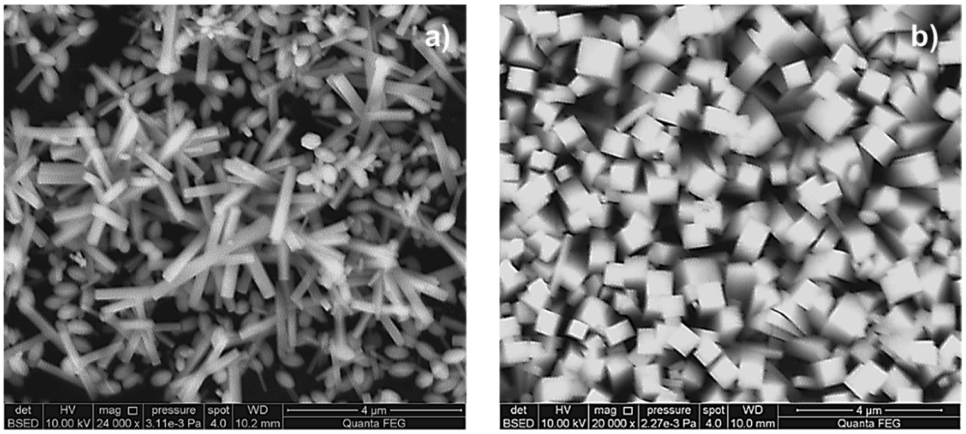

Fig. 16. SEM image of (a) thin and (b) thick subsurface covered layer.

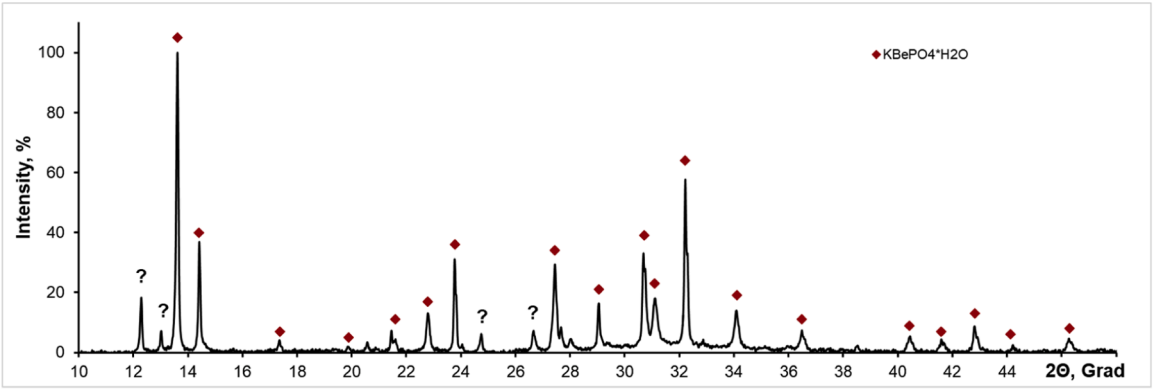

Fig. 17. X-ray diffraction pattern of surface layer formed on Be foils after 120 days of corrosion in MPC pore water.

apparently determines the needle-like shape of the crystals formed. This phase was also found in similar investigations on beryllium corrosion in MPC solutions [14]. No reflexes corresponding to the crystalline beryllium hydroxide were detected in the XRD patterns. Apparently, $Be(OH)_2$ is present in the corrosion product layer, but its amount is insignificant, and it is probably amorphous as reported in [16,13,14]. Several reflexes (Fig. 17, question mark) could not be identified as either beryllium oxides or hydroxides, or as other phosphate phases. Further experimental study is needed to clarify the composition of this corrosion product/precipitate.

Thus, the content of beryllium in the cover layer can be determined from the ratio of the molecular weights of beryllium (9.0122 g/mol) and $BeKPO_4{\cdot}H_2O$ compound (161.1009 g/mol).

$$m_{Be}^{covL} = 0.05594 M_{covL} \quad (7)$$

The mass of corroded beryllium consists of three components: the mass of Be as hydroxide on the metal surface m_{Be}^{s}, dissolved in solution (m_{Be}^{sol}) and beryllium included in the cover layer (m_{Be}^{covL}).

$$m_{Be}^{cor} = m_{Be}^{s} + m_{Be}^{sol} + m_{Be}^{covL} \quad (8)$$

Using Eqs. (2) and 8, the expression for the mass of corroded beryllium metal can be obtained (Eq. (9)), which consists of two experimentally measured values, namely the concentration of beryllium in solution (determined by ICP-MS) and weight loss (WL*), and analytically determined beryllium content in the coating layer (Eqs. (6) and 7).

$$m_{Be}^{cor} = \frac{R\left(m_{Be}^{sol} + m_{Be}^{covL}\right) + WL^{*}}{R-1} \quad (9)$$

It can be seen, when no covering layer ($m_{Be}^{covL} = 0; WL^{*} = WL$) is observed, Eq. (9) is transformed into Eq. (4).

Based on this method (Eq. (9)), the corrosion rates (CR) were calculated for MPC and MPC + *B* solutions, and the results are presented in Fig. 18. The corrosion rates are 2.06 ± 0.04 μm/y and 1.02 ± 0.02 μm/y for the MPC and MPC+*B* pore water, respectively. It can be seen that even small additions of boric acid to MPC pore water significantly (2 times) reduce the corrosion rate of beryllium. In the MPC experiments, the accumulating dissolved beryllium reaches saturation of the solution with respect to $BeKPO_4$ and the relative precipitation and Be dissolution rates may become coupled and establish an overall steady state rate.

Finally, the results of measurements of the beryllium corrosion rates for OPC, MPC, MPC+*B* pore water solutions and for NaOH based solutions with similar pH are summarized in Table 4.

It can be seen that after a test duration of four months, the corrosion rate is comparable for OPC and MPC solutions, despite the significant difference in pH. The addition of boric acid to the MPC- solution reduces the corrosion rate by half, although the decrease in pH is insignificant. The minimum corrosion rate is observed for an aqueous solution with a pH of 6.7.

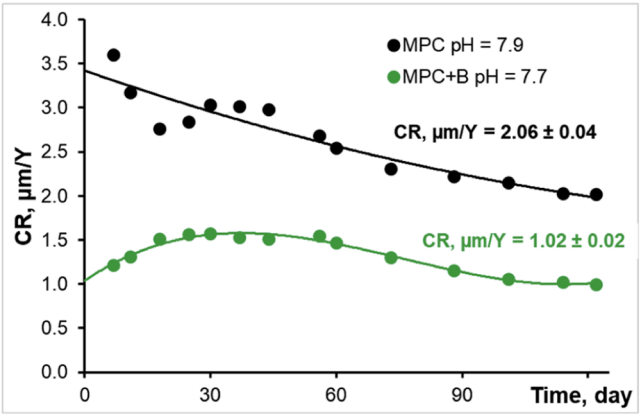

Fig. 18. Corrosion rate of Be in MPC and MPC+*B* pore water as a function of exposure time.

Table 4
Corrosion rates (CR) of metallic beryllium in OPC, MPC, MPC + *B* and NaOH solutions.

Medium	pH	CR, μm/y	
		30 days	122 days
NaOH	6.7	0.16 ± 0.01	0.040 ± 0.002
NaOH	13.4	5.7 ± 0.2	2.8 ± 0.1
OPC	13.4	4.8 ± 0.2	1.90 ± 0.09
MPC	7.9	2.96 ± 0.05	2.06 ± 0.05
MPC + B	7.7	1.55 ± 0.01	1.02 ± 0.02

3.3. Comparative analysis of beryllium corrosion in various media

The results of all our corrosion rate measurements (duration 30 days) in different aqueous solutions are summarized in Fig. 19. Under alkaline conditions (green points, pH > 12), the corrosion rates of beryllium in logarithmic coordinates increase linearly with increasing pH.

$$Log(CR_{Be}) = 2.064pH - 26.782 \quad (10)$$

A similar linear dependence for metallic aluminum was obtained on the basis of our previous experimental data [15] and is equal to:

$$Log(CR_{Al}) = 0.972pH - 8.359 \quad (11)$$

Comparing these two dependencies shows that the corrosion rates of metallic aluminum are 3 to 4 orders of magnitude higher than those of beryllium. For example, for pH values of 12.5 and 14, the ratio of corrosion rates (CR_{Al}/CR_{Be}) for metallic aluminum and beryllium is 5.9×10^4 and 1.4×10^3, respectively. This indicates that metallic aluminum

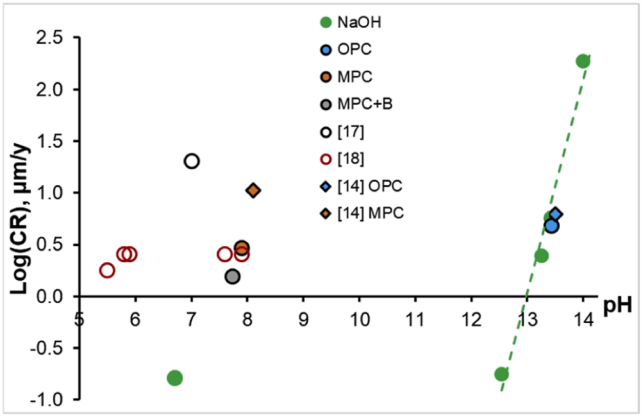

Fig. 19. Corrosion rates of metallic Be in various solutions.

is not a suitable analogue to assess the behavior of beryllium under highly alkaline conditions.

The literature data on beryllium corrosion in various media are presented in Fig. 19 for comparison. For all our and the literature data, the corrosion rate was measured using direct methods, such as mass loss, ICP-MS and hydrogen release, and the duration of corrosion experiments was approximately 30 days.

It should be noted that these literature data [17,18] for neutral and slightly acidic solutions are the estimations of the corrosion rates rather than accurately measured values. English [18] reported that corrosion rate remains constant in a wide pH region (from pH = 4 to pH = 8) and equals 2.54 µm/y. In the present work, the measured value of corrosion rate at pH = 6.7 is lower and equals 0.16 µm/y. This difference could be explained by the different temperatures used in the corrosion experiments. In our study corrosion experiments were conducted at room temperature, while in [18] at 80 °C. In the work of Prochko et al. [17], for experiments in distilled water at 16 °C, the measured corrosion rate is significantly higher (20.8 µm/y) than that obtained in [18] and in our experiments. This can only be explained by the fact that beryllium (98.3 % purity) with a high content of impurities was used in [17], which enhances the corrosion.

The corrosion rate of beryllium in OPC pore water (Fig. 19, blue point, pH = 13.4) is slightly lower than in NaOH based solution (green point, pH = 13.4) and it is also well described by this straight line (Eq. (10)). In addition, our experimental data correlate well with the results (blue diamond point, pH = 13.5) reported in [14], which were measured by another direct method, namely by measuring the hydrogen release.

Experimental data on beryllium corrosion in MPC pore solution after 30 days determined recently by Caes et al. [14] are higher than our data, 10.5 µm/y (brown diamond) and 2.96 µm/y (brown circle), respectively (Fig. 19). In [14] S-200-F grade metallic beryllium with a purity of 98.5 % was used, whereas we used beryllium with a purity of 99.8 %. Therefore, the differences in corrosion rates between our present study and [14] is likely to be due to the different purities of the beryllium used. However, other factors such as differences in the beryllium metal microstructure and/or surface finish cannot be excluded.

It should be particularly noted that despite the large difference in the pH of the solutions, the difference between the corrosion rates in OPC and MPC solutions (after 122 days) is quite small: 1.90 µm/y and 2.06 µm/y, respectively, see Table 4. Small additions of boric acid to MPC pore water further reduce the corrosion rate by half to 1.02 µm/y.

Finally, the Be concentration in solution was measured after 30 days of corrosion for all studied conditions. Cannes et al. [13] previously reported the solubility diagram of Be(II) species as a function of the pH. They showed that solid $Be(OH)_2$ can dissolve into 6 different forms depending on the pH of the system. The diagram reveals also that the solubility limit of solid $Be(OH)_2$ is the lowest in pH between 8.2 and 10.5, while it increases at pH ⟨ 8.2 or pH ⟩ 10.5. This means that the corrosion product layer is stabilized faster at near neutral pH than at more acidic/basic pH. To corroborate this diagram with the corrosion tests done in this study, Be concentrations measured in the solutions were reported in the solubility diagram (Fig. 20). All concentrations fall very close to the limit of solubility of $Be(OH)_2$, proving that after 30 days of corrosion, the solid $Be(OH)_2$ corrosion product layer is already formed in all systems and should thicken at the surface of the metal as the with time.

4. Conclusions

In the present work, the corrosion behavior of metallic beryllium in sodium hydroxide solutions with pH ranging from 6.7 to 14.0 and in solutions simulating potential encapsulation matrices such as Ordinary Portland Cement (OPC) or magnesium phosphate cement (MPC) was examined in detail by various physico-chemical methods. The main conclusions are as follows:

1. A combined method is proposed based on these two direct methods, namely, measurements of weight loss of the initial samples (WL) and the concentration of beryllium in solution (determined e.g. by ICP-MS) and taking into account the formation of a thin layer of beryllium hydroxide on the sample surface during corrosion. It should be particularly noted that the proposed combined method permits to determine the corrosion rates of beryllium in solutions with near neutral to alkaline pH values (6.7 and 12.5) when the change in the mass of the sample is close to zero or even positive, i.e., even in cases where measuring the corrosion rate solely by the WL method is impossible.
2. Under highly alkaline conditions at pH > 12, the corrosion rates of beryllium in logarithmic coordinates increase linearly with increasing pH: $Log(CR_{Be}) = 2.064pH - 26.782$.
3. Detailed SEM studies of the material before and after corrosion tests suggest pitting corrosion as one important mechanism of beryllium metal corrosion at highly alkaline conditions. Two types of corrosion pits were observed in the corroded samples: large (40 – 200 µm) and small (4 – 30 µm) pits. The total size distribution of corrosion pits consists of the sum of two lognormal distributions corresponding to large and small pits. The total number of corrosion pits increases monotonously with increasing pH. This increase is mainly determined by an increase in the number of small corrosion pits, whereas the number of large corrosion pits increases only slightly.
4. The large corrosion pits are formed at all pH values of the solutions. Their size and quantity change slightly with increasing pH. Therefore, it can be assumed that the formation of large corrosion pits occurs mainly on cavities and on large scratches that are present in the original beryllium foil.

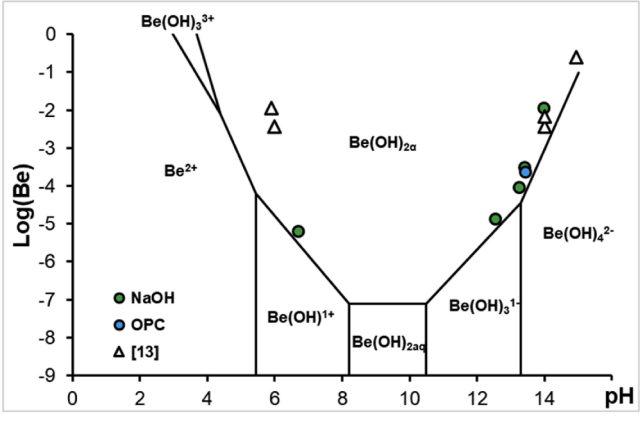

Fig. 20. Solubility diagram of Be species as function of the pH [13].

5. Large corrosion pits are not hemispherical and have an irregular shape with a complex internal morphological structure. The pits consist of several special areas with differently oriented parallel plates. It was confirmed that the size of the special areas is determined by the grain size of the initial Be metal.
6. The corrosion process of metallic beryllium in MPC and MPC + *B* pore water solutions are accompanied by the formation of an additional black or grey material layer on the surface of the samples. The detail SEM analyses showed that this layer consists mainly of randomly oriented needle-like crystals. Detailed X-ray diffraction analyses revealed that the cover layer consists mainly of BeKPO4·H2O.
7. The presented combined method to determine the corrosion rate based on the two direct methods was developed considering the formation of a thin layer of BeKPO4·H2O on the sample surface during corrosion.
8. It should be particularly noted that despite the large difference in solution pH, the difference between the corrosion rates in OPC and MPC solutions is quite small: 1.90 μm/y and 2.06 μm/y, respectively, revealing no distinct benefit of encapsulating radioactive beryllium metal waste in MPC instead of OPC. Small additions of boric acid to MPC pore water distinctly decrease the corrosion rate down to 1.02 μm/y. However, it should be noted that the determined corrosion rates refer to the particular experimental conditions and cannot directly be used for performance assessment of encapsulated beryllium wastes under storage or disposal conditions, where the limited supply of pore water is affecting the corrosion rates. This topic will be subject of further research.

Funding

Open Access funding enabled by the Deutsche Forschungsgemeinschaft (DFG, German Research Foundation) – 491111487 and organised by the Projekt DEAL.

Data availability The data generated during the current study are available from the corresponding author on reasonable request.

Appendix A. supplementary data

Supplementary material related to this article can be found, in the online version,

CRediT authorship contribution statement

Andrey Bukaemskiy: Writing – review & editing, Writing – original draft, Validation, Methodology, Investigation, Conceptualization. **Guido Deissmann:** Writing – review & editing, Validation, Supervision. **Sebastien Caes:** Writing – review & editing, Investigation. **Giuseppe Modolo:** Writing – review & editing, Validation, Supervision. **Dirk Bosbach:** Writing – review & editing, Supervision, Funding acquisition.

Declaration of competing interest

The authors declare that they have no known competing financial interests or personal relationships that could have appeared to influence the work reported in this paper.

Acknowledgements

This project has received funding from the Euratom research and training programme 2014-2018 under grant agreement No 945098 (PREDIS).

Data availability

Data will be made available on request.

References

[1] B.G. Naik, N. Sivasubramanian, Applications of beryllium and its alloys, Miner. Process. Extr. Metall. Rev. 13 (1994) 243–251, https://doi.org/10.1080/08827509408914113.
[2] G.R. Longhurst, K. Tsuchiya, C.H. Dorn, S.L. Folkman, T.H. Fronk, M. Ishihara, H. Kawamura, T.N. Tranter, R. Rohe, M. Uchida, E. Vidal, Managing beryllium in nuclear facility applications, Nucl. Technol. 176 (2011) 430–441, https://doi.org/10.13182/NT11-A13318.
[3] ed. by K. Kurosaki, S. Yamanaka, Neutron reflector materials (Be, hydrides), in: R. J.M. Konings, R.E. Stoller (Eds.), Comprehensive Nuclear Materials, 2nd Edition, Elsevier, Amsterdam, 2020, pp. 382–399, https://doi.org/10.1016/B978-0-12-803581-8.11747-3. ed. by.
[4] ed. by G. Federici, R. Doerner, P. Lorenzetto, V. Barabash, Beryllium as a plasma-facing material for near-term fusion devices. Chapter 4.19, in: R.J.M. Konings (Ed.), Comprehensive Nuclear Materials, Elsevier, Amsterdam, 2012, pp. 621–666, https://doi.org/10.1016/B978-0-08-056033-5.00121-X. ed. by.
[5] ed. by M. Nakamichi, J.-H. Kim, M.M. Nakamura, T. Shibayama, C.K. Dorn, C. Vladimir, D.V. Bachurin, C. Stihl, P.V. Vladimirov, Beryllium and its alloys as neutron multiplying materials, in: R.J.M. Konings, R.E. Stoller (Eds.), Comprehensive Nuclear Materials, 2nd Edition, Elsevier, Amsterdam, 2020, pp. 203–250, https://doi.org/10.1016/B978-0-12-803581-8.11673-X. ed. by.
[6] J.S. Park, X. Bonnin, R. Pitts, Assessment of ITER divertor performance during early operation phases, Nucl. Fusion. 61 (2021) 016021, https://doi.org/10.1088/1741-4326/abc1ce.
[7] J.M. Marder, Beryllium – technology and applications, JOM 36 (1984) 45–47.
[8] ed. By F. Glasser, in: M.I. Ojovan (Ed.), Handbook of Advanced Radioactive Wastes Conditioning Technologies, Woodhead, 2011, pp. 67–135, https://doi.org/10.1533/9780857090959.1.67. ed. By.
[9] C. Cau Dit Coumes, D. Lambertin, H. Lahalle, P. Antonucci, C. Cannes, S. Delpech, Selection of a mineral binder with potentialities for the stabilization/solidification of aluminum metal, J. Nucl. Mater. 453 (2014) 31–40, https://doi.org/10.1016/j.jnucmat.2014.06.032.
[10] S. Delpech, C. Cannes, N. Barré, Q.T. Tran, C. Sanchez, H. Lahalle, D. Lambertin, S. Gauffinet, C. Cau-dit-Coumes, Kinetic model of aluminum behavior in cement-based matrices analyzed by impedance spectroscopy, J. Electrochem. Soc. 164 (2017) C717–C727, https://doi.org/10.1149/2.0211713jes.
[11] R. Perona, C. Fernández-García, I. García-Lodeiro, M. Criado, J.M. Bastidas, M. C. Alonso, Corrosion behavior and immobilization of pure aluminum and Al−Mg alloy LLRW in magnesium potassium phosphate cements, J. Nucl. Mater. 582 (2023) 154501, https://doi.org/10.1016/j.jnucmat.2023.154501.
[12] P. Bouhier, C. Cannes, Lambertin D, C. Grisolia, D. Rodrigues, S. Delpech, Evaluation of several conditioning matrices for the management of radioactive metal beryllium wastes, J. Nucl. Mater. 559 (2022) 153464, https://doi.org/10.1016/j.jnucmat.2021.153464.
[13] C. Cannes, P. Bouhier, D. Lambertin, C. Grisolia, D. Rodrigues, S. Delpech, Reactivity of beryllium in aqueous solution from acidic to basic pH, J. Electroanal. Chem. 950 (2023) 117879, https://doi.org/10.1016/j.jelechem.2023.117879.
[14] S. Caes, A. Bukaemskiy, C. Cannes, S. Delpech, V. De Sousa, B. Kursten, Study of the behaviour of beryllium in solutions representative of OPC and MPC cementitious materials, J. Nucl. Mater. 616 (2025) 156023, https://doi.org/10.1016/j.jnucmat.2025.156023.
[15] A. Bukaemskiy, S. Caes, G. Modolo, G. Deissmann, D. Bosbach, Investigation of kinetics and mechanisms of metallic beryllium corrosion for the management of radioactive wastes, MRS Adv. 9 (2024) 391–396, https://doi.org/10.1557/s43580-024-00835-y.
[16] K.A. Walsh, Beryllium Chemistry and Processing, ASM International, Materials Park, 2009.
[17] R.J. Prochko, J.R. Myers, R.K. Saxer, Corrosion of beryllium by salt water, Mater. Prot. 5 (1966) 39–42.
[18] J.L. English, The Metal Beryllium, American Society for Metals, Cleveland, 1955.
[19] M.A. Hill, D.P. Buft, R.S. Litlard, The passivity and breakdown of beryllium in aqueous solutions, J. Electrochem. Soc. 145 (1998) 2799–2806, https://doi.org/10.1149/1.1838717.
[20] E. Gulbrandsen, A.M.J. Johansen, A study of the passive behavior of beryllium in aqueous solutions, Cor. Sci. 36 (9) (1994) 1523–1536, https://doi.org/10.1016/0010-938X(94)90050-7.
[21] R.U. Vaidya, M.A. Hill, M. Hawley, D.P. Butt, Effect of pitting corrosion in NaCl solutions on the statistics of fracture of beryllium, Met. Mat. Trans. A 29A (1998) 2755.
[22] J.R. Friedman, J.E. Hanafee, Corrosion/electrochemistry of monocrystalline and polycrystalline beryllium in aqueous chloride environment, UCRL-ID-137482, 2000.
[23] R.S. Lillard, Factors influencing the transition from metastable to stable pitting in single-crystal beryllium, J. Electrochem. Soc. 148 (2001) B1–B11, https://doi.org/10.1149/1.1344526.
[24] J.S. Punni, M.J. Cox, The effect of impurity inclusions on the pitting corrosion behaviour of beryllium, Cor. Sci. 52 (2010) 2535–2546, https://doi.org/10.1016/j.corsci.2010.03.024.
[25] J.S. Punni, Electrochemical characterization to study the pitting corrosion behaviour of beryllium. Pitting Corrosion, 2012. ISBN 978-953-51-0275-5.
[26] R.W.G. Wyckoff, Crystal Structures Vol. 1, Interscience Publishers, New York, 1963.

[27] Laboratory immersion corrosion testing of Metals1, ASTM–G31–12a.
[28] R. Stahl, C. Jung, H.D. Lutz, W. Kockelmann, H. Jacobs, Z. Anorg, Kristallstrukturen und Wasserstoffbrückenbindungen bei β-$Be(OH)_2$ und ϵ-Zn $(OH)_2$, Allg. Chem. 624 (1998) 1130–1136, https://doi.org/10.1002/(SICI)1521-3749(199807)624:7<1130::AID−AAC1130>3.0.CO;2-G.
[29] J.M. West, Electrodeposition and Corrosion Processes, Plenum Press, New York, 1970.